Journal of Materials Chemistry C

Accepted Manuscript

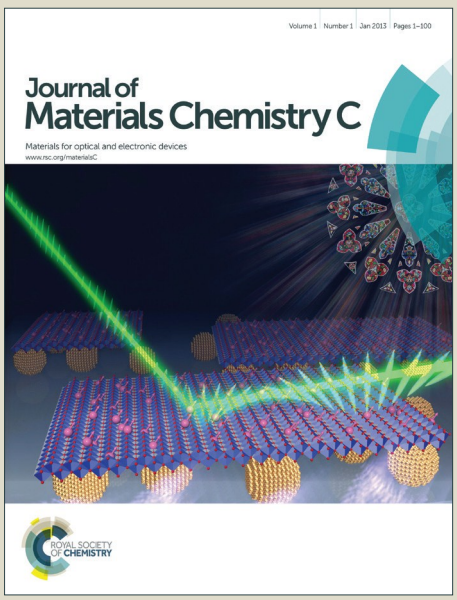

ROYAL SOCIETY OF CHEMISTRY

www.rsc.org/materialsC

Journal Name

RSCPublishing

ARTICLE

In situ synthesis of highly crystalline Tb-doped YAG nanophosphor using the mesopores of silica monolith as template

Cite this: DOI: 10.1039/x0xx00000x

Received 00th January 2015,
Accepted 00th January 2015

DOI: 10.1039/x0xx00000x

www.rsc.org/

Abdelhay Aboulaich[1,2], Nathalie Caperaa[1,2], Hicham El Hamzaoui[3], Bruno Capoen[3], Audrey Potdevin[2,4], Mohamed Bouazaoui[3], Geneviève Chadeyron*[2,4], Rachid Mahiou[1,2]

This report describes the first synthesis of highly crystalline YAG:Tb nanophosphor inside the pores of Mesoporous Silica Monolith (MSM). A simple wet impregnation procedure using YAG:Tb sol and MSM platform prepared by sol-gel method was adopted to prepare highly homogeneous MSM-YAG:Tb luminescent composite. The morphological, structural and luminescent properties of *in situ* generated YAG:Tb nanocrystals, investigated using XRD, TEM, HRTEM, EDS, FTIR, nitrogen gas sorption and photoluminescence measurements, were compared to those of bulk YAG:Tb phosphor. The specific surface area and pore volume of MSM host material were found to be lower when YAG:Tb nanoparticles were grown in the pores of MSM material. The particle diameter of nano-sized YAG:Tb phosphor was estimated to be about 23 nm. MSM-YAG:Tb composite exhibited a strong green fluorescence emission with the characteristic main emission band of Tb^{3+} located at 547 nm. The prepared composite also showed shorter photoluminescence (PL) lifetime and excitation bands shifted to lower wavelengths compared to the neat YAG:Tb phosphor. The as-prepared MSM-YAG:Tb material could be integrated into optoelectronic devices and holds a good potential to be applied in decorative lighting.

Introduction

Rare earth-doped phosphors (RE-phosphors) attract more and more attention with the continuous emergence of novel and attractive applications in addition to their potential applications in many optoelectronics devices such as light-emitting diodes (LEDs), solid state lasers, optical fibre amplifiers and solar devices.[1] Among these applications, phosphors-converted LEDs (pc-LEDs) have been extensively investigated during the last few decades due to their potential applications in solid-state lighting and display systems. The great interest in pc-LEDs arises from their unique properties including but not limited to low power consumption, smaller volume, long lifetime and smaller environmental impact compared with conventional lighting systems.[2-4] In recent years, pc-LEDs have been broadly applied to screens, traffic lights, automobile lights, LCD backlight, white lighting sources, lighting sources for special purposes, decorative luminaires, *etc*.

RE-phosphors with large particle size (1-20 μm) are typically combined with LED and used as down-converting materials to efficiently convert blue or UV light from LED into visible light with longer wavelength. The best-known pc-LED is based on the association of the widely used Ce-doped Yttrium Aluminium Garnet $Y_3Al_5O_{12}$ (YAG:Ce) phosphor with a blue LED to create a white light by combining yellow light from the phosphor with a blue light from GaN-based LED. RE-phosphors are generally mixed with encapsulant materials, typically with polymeric matrices, and then applied to LED chip as coating or films.[5] Although, LEDs-based lighting offers many advantages over conventional lighting, on average LED lamps remain more expensive than other lighting technologies. One possible way to reduce the packaged pc-LED cost consists in reducing the phosphor cost and/or the required amount of the phosphor, which represents about 12% of the total manufacturing cost of packaged pc-LED according to the report published by U.S. Department of Energy in

September 2013.[6] In this context, it has been proved in several studies that pc-LEDs using phosphors with smaller particle size and narrower grain size distribution, required a lower amount of phosphor to get efficiency similar to LEDs using phosphor with bigger particles.[7, 8] This could potentially save cost of pc-LEDs. Other advantage of phosphors with small particle size, and more especially nanophosphor, is that the rare earth doping species in the host material are homogeneously distributed compared to bulk phosphor during their synthesis. This is because nanophosphors are generally prepared at low temperature synthesis starting from molecular precursors in solution yielding highly quality phosphors materials since mixing and doping uniformity is easy to achieve at molecular scale. [9,10] Unlike nanophosphors, bulk phosphor materials are generally prepared, at higher temperatures synthesis using solid state reaction, starting from larger size precursors (typically oxides-based precursors), which generally results in lower degree of homogeneity, particularly with regard to rare earth doping. Thus, energy transfer between the luminescence centres within RE-nanophosphors is reduced due to well separated rare-earth dopants in each nanophosphors and, as a result, concentration quenching would be suppressed for nanosized phosphors.[11]

Consequently, research on nanophosphors has attracted broad interest for use in pc-LEDs in the past few decades.[9, 12-18] Otherwise, the development of new processes allowing to produce encapsulating materials and supports for nanophosphors materials with a high and easy control of the final macroscopic shape (including size and morphology) is now of great interest especially for decorative lighting. For this purpose, Mesoporous Silica Monoliths (MSM) might be a potential candidates because of their unique properties as rigidity, high surface area, tuneable pore diameter, photo/thermal and chemical stability.[19] Indeed, the high surface area and tuneable pore diameter provided by mesoporous silica matrices should allow to better disperse the RE-nanophosphor with narrow size distribution and achieve highly homogeneous nanophosphor/silica optical material. In addition, the control of shape and size of the final MSM can be easily achieved by using the suitable shaped-recipient during the gelation/consolidation stage of the process. These features should enable new LED lighting devices designed for decorative purposes while reducing the required amount of the phosphor.

Ordered mesoporous silica sieves like MCM41 and SBA15 have been widely used as host matrices for various luminescent materials including rare earth complexes, rare earth metal oxides, rare earth fluorides, dye molecules and quantum dots.[20-32]

However, ordered mesoporous silica sieves require relatively expensive surfactants and triblock copolymers (*e.g.* P123, F127) used as structure-directing agents. Furthermore, it is often difficult to prepare bulk materials from those ordered silica sieves. Silica xerogels with tuneable pore diameter have also been synthesized, using alkoxides-based sol-gel method, to yield stable bulk silica monoliths without using any structure-directing agents.[31] These materials may have more commercial potentials because of using low-cost and widely available silica precursors and reactants.

Mesoporous silica embedded with luminescent compounds can be prepared by using several approaches. One approach consists in introducing the luminescent material in silica matrix during the early stages of preparation by using co-condensation method. This one-step synthesis method yields stable hybrid luminescent materials with strong interaction (usually with covalent bonds) between the host silica framework and luminescent compounds, thus reducing the leaching of guest compounds from the silica matrix.[31] However, it is recognized that the difference in reaction rates between silica and guest precursors might lead to non-homogeneous dispersion of luminescent compounds and thus phase separation can occur.[21] In addition, a decrease in emission intensity is often observed in the final hybrid material compared to the pure luminescent material.[29] The second approach is based on the incorporation of luminescent compounds once the silica framework is formed. This method has been widely used for *in situ* synthesis of a large number of metal oxides and semiconductor nanoparticles in the pores of mesoporous silica.[33-36] However, very few reports are available on the *in situ* synthesis of RE-nanophosphors, especially RE-doped YAG nanophosphors, inside the pores of MSM. Among RE-doped YAG, Tb^{3+}-doped YAG (YAG:Tb) phosphor has been extensively studied due to its well-known green emission, which can be efficiently sensitized by means of several sources such as cathode-ray, VUV, UV and low-voltage excitations.[37]

Herein, we report the first *in situ* synthesis of YAG:Tb nanocrystals inside the pores of MSM using a simple wet impregnation procedure followed by a calcination stage to get a highly crystalline YAG phase. For comparison purposes, YAG:Tb crystalline powder was also prepared in the same conditions as MSM-YAG:Tb nanocomposite.

Experimental section

Synthesis of Mesoporous Silica Monolith (MSM):

Monolithic porous silica matrices were prepared following the procedure already reported[38] This sol-gel process yields a large range of mesoporous xerogels with interconnected pores and a well-controlled pore size distribution. In this paper, we

consider silica xerogels with a mean pore size of 24 nm. These xerogels were obtained by hydrolysis and polycondensation of tetraethylorthosilicate (TEOS), followed by a drying step and stabilization in air at 1000 °C.

Synthesis of YAG:Tb sol:

YAG:Tb (20 mol %) sol was prepared according to the method already detailed in our previous reports.[37, 39] Anhydrous yttrium chloride YCl_3 (99.99% pure, Aldrich), terbium chloride $TbCl_3$ (99.99% pure, Aldrich), metallic potassium (98% pure, Aldrich), aluminium isopropoxide (99.99+% pure, Aldrich) and anhydrous isopropanol (iPrOH, 99.8+% pure, Aldrich) have been used as starting materials. The synthesis consists in preparing separately a solution A of anhydrous yttrium and terbium chlorides dissolved in anhydrous isopropanol and a solution B of potassium isopropoxide. Solution B is slowly added to solution A under vigorous stirring: a precipitate of KCl appears immediately. The mixed solution is maintained at 85°C during 1 h. Then, a known quantity of aluminium isopropoxide powder is poured directly into the A/B mixture. After further reflux for 4 h at 85°C, a clear and homogeneous solution (solution C) is obtained together with the KCl precipitate. This latter is removed by centrifugation after cooling. The centrifugation step was repeated three times in order to make out all traces of KCl salts. The obtained clear supernatant corresponds to the YAG:Tb sol.

***In situ* synthesis of YAG:Tb nanocrystals into the pores of Mesoporous Silica Monolith (MSM-YAG:Tb):**

MSM was dried under vacuum for 12 h at 100°C before use. YAG:Tb nanocrystals were synthesized in the pores of MSM using a simple wet impregnation process. In a typical procedure, a dried MSM was immediately placed in YAG:Tb sol for 72 h. To complete the pores filling, the imbibed MSM was then dried in oven at 80°C under vacuum for 12 h and then placed again in YAG:Tb sol for 10 min. The 10 min impregnation process was repeated 10 times. Each impregnation step is followed by a drying step at 80°C for 15 min to remove the isopropanol solvent. The imbibed MSM was finally sintered at 1100°C for 4 h to let the YAG:Tb crystals grow inside the mesopores of silica matrix. This material will be named MSM-YAG:Tb in the next part of this report. The *in situ* preparation process of YAG:Tb nanocrystals in the pores of MSM is illustrated in scheme 1.

In order to quantify the amount of YAG:Tb nanocrystals loaded in the silica monolith, silica template was removed from the MSM-YAG:Tb nanocomposite using an aqueous solution of NaOH (1 M). A sample of MSM-YAG:Tb was immersed in the basic solution and heated at 55°C overnight with vigorous stirring. After silica dissolution, the YAG:Tb nanocrystals were subsequently collected as a powder by centrifugation (10000 rpm/10 min).

Synthesis of YAG:Tb crystalline powder :

To conduct a comparative study, we separately prepared YAG:Tb crystalline powder. YAG:Tb sol was hydrolyzed by introducing an excess of water, resulting in transparent gel, which was further dried at 80◦C to yield a white xerogel. The later was sintered at 1100°C for 4 h in a muffle furnace in order to obtain well-crystallized YAG:Tb phosphors powder.

Characterization:

The XRD measurements were performed using a Philips Xpert Pro diffractometer using Cu Kα radiation with a wavelength of 1.5406Å. Transmission Electron Microscopy (TEM) images were taken by grinding a small piece of MSM-YAG:Tb monolith into powder and by depositing the powder onto a carbon film-supported copper grid. Samples were studied using a FEI Tecnai G2 20 instrument operating at 200 kV. In order to characterize the porosity of MSM and MSM-YAG:Tb, nitrogen sorption isotherms were recorded at 77.35 K using a Quantachrome porosimeter Autosorb 1-LP-MP, after an outgassing process of several hours at 150°C under secondary vacuum. Specific surface area was determined by the Brunauer–Emmett–Teller (BET) method.[40] The pore size distribution was obtained from the desorption isotherm using the Barrett–Joyner–Halenda (BJH) model.[41] Photoluminescence (PL) emission and excitation features, as well as absolute photoluminescence quantum yield (PL-QY) values, were measured using a C9920-02G PL-QY measurement system from Hamamatsu. The setup comprises a 150 W monochromatized Xe lamp, an integrating sphere (Spectralon Coating, Ø = 3.3 inch) and a high sensitivity CCD spectrometer for detecting the whole spectral luminescence. Photoluminescence Excitation (PLE) spectra were obtained by exciting the samples from 250 to 400 nm with 3 nm increment and measuring their absolute PL QY by monitoring the overall emission of the samples in the 400-700 nm wavelength range. Absolute QY values were then used and combined with the absorption coefficient (also measured by the apparatus) to plot the excitation spectra. The PL decays were obtained using a pulsed dye laser (Continuum ND60) pumped by a frequency doubled pulsed YAG:Nd^{3+} laser (continuum surelite I) with 10 ns pulse, 0.1 cm^{-1} band-width and 10 Hz repetition rate. The dye laser was followed by a KDP frequency doubler. The UV beam is isolated from the fundamental dye laser beam by a Pellin-Broca prism

associated with iris diaphragm and UV Bandpass filter UG-11. Rhodamine 590 used as dye solution provided energy up to 400 µJ in the doubled selected UV region. Fluorescence decays were then measured with a LeCroy 400 MHz digital oscilloscope.

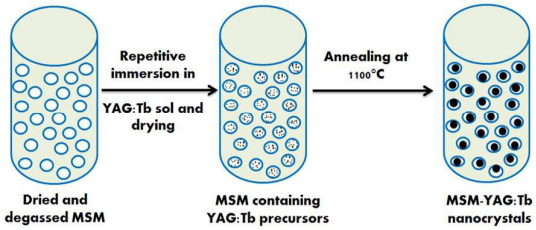

Scheme 1. Schematic illustration of the *in situ* formation of YAG:Tb nanocrystals in the pores of MSM

Results and discussion:

The N_2 adsorption/desorption isotherms and pore-size distributions of as-prepared MSM before loading with YAG:Tb precursors are shown in Figure 1.

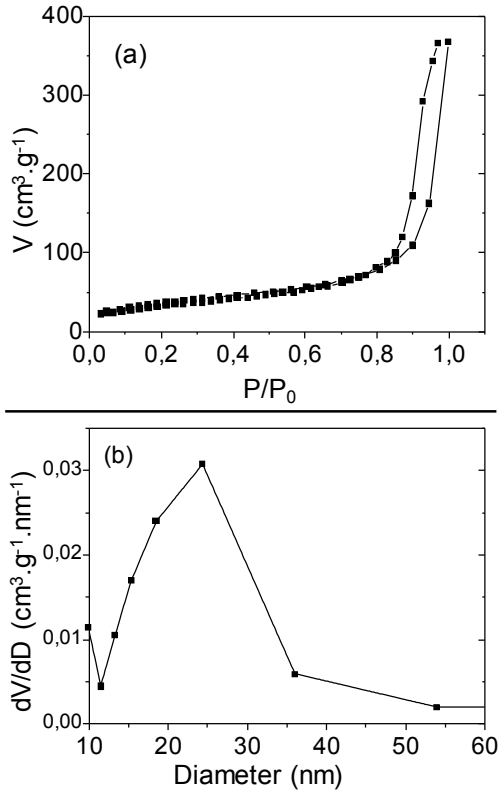

Figure 1. (a) N_2-sorption isotherm and (b) BJH pore size distribution of as-prepared MSM.

From Figure 1(a), it can be seen that MSM host have a IV type isotherm with H_2 hysteresis loop according to the IUPAC classification, which is characteristic of mesoporous materials with interconnected pores. The pore size distribution is given by the derivative of the desorbed volume as a function of the pore diameter (Fig.1(b)). MSM material exhibited interconnected pores with an average diameter of 24 nm. The specific surface area was found to be around 130 $m^2.g^{-1}$. The total pore volume, measured at the highest relative pressure (P/P_0), is 0.57 $cm^3.g^{-1}$ (Table 1). Compared to the non-embedded MSM, MSM-YAG:Tb composite showed much lower specific surface area and pore volume. The drop in specific surface area (by about 54%) and pore volume (by about 80%) within the MSM-YAG:Tb material is in agreement with an efficient pores filling with YAG:Tb phosphor by using our wet impregnation procedure. The silica template was successfully removed from the composite using concentrated NaOH solution as described in the experimental section. It was found that YAG:Tb content in the composite represents about 10-15 wt% relative to the silica.

Sample	Specific surface area ($m^2.g^{-1}$)	Pore volume ($cm^3.g^{-1}$)
MSM	130	0.57
MSM-YAG:Tb	60	0.1

Table 1. Specific surface area and pore volume of MSM and MSM-YAG:Tb materials

The MSM annealed at 1100°C for 4 h, MSM-YAG:Tb and YAG:Tb powder have been characterized using XRD. The resulting patterns (figure 2) show that MSM-YAG:Tb and YAG:Tb powder are crystallized while the neat MSM annealed at the same temperature is amorphous. All diffraction peaks for both MSM–YAG:Tb and YAG:Tb powder are assigned to the YAG structure (JCPDS-file 33-0040). XRD pattern of MSM-YAG:Tb also shows a broad component at about 20° attributed to the amorphous silica matrix.

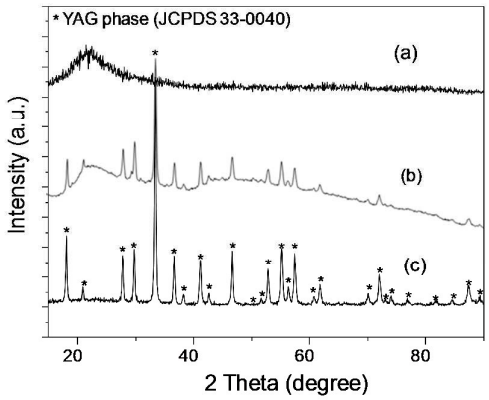

Figure 2. XRD patterns of (a) MSM annealed at 1100°C/4h, (b) MSM-YAG:Tb and (c) YAG:Tb powder

In first approximation, the average crystallite size has been determined from the full-width at half maximum (FWHM) of the diffraction peaks using Scherrer's equation : $\langle D \rangle = k\lambda/\beta\cos\theta$, where D is the mean particle size, k is a geometric factor (here, k = 0.9),[42] λ is the X-Ray wavelength (1.5406 Å), and β is the corrected half-width of the selected diffraction peak located at about 33°(2 θ). Estimated from the formula, the average crystallite sizes of the *in situ* prepared YAG:Tb particles are about 23 nm. This crystallite size matches well the pore diameter of MSM, thus indicating that YAG:Tb nanocrystals are mainly formed inside the pores of the mesoporous material. To the best of our knowledge, this is the first demonstration of YAG:Tb nanophosphor synthesis using the pores of MSM as nanoreactors.

The morphological and structural properties as well as the chemical composition of MSM-YAG:Tb composite were also investigated using TEM and HR-TEM analyses coupled with EDS measurements (figure 3). TEM image in dark field mode (Figure 3(b)) reveals the coexistence of bright (*i.e.* diffracting zones) and dark areas (*i.e.* non-diffracting zones) corresponding to crystalized and amorphous areas, respectively. Moreover, EDS analysis performed on a whole powder grain (figure 3(c)) shows the coexistence of a small amount of YAG:Tb in a matrix logically dominated by silica while EDS spectrum from strongly crystallized areas shows YAG:Tb enriched composition of these zones of few tens of nanometers. In addition, bright areas seem to be relatively well distributed within the amorphous enriched silica zones, indicating a relatively high homogeneous dispersion of crystallized YAG:Tb in the MSM host material. The HR-TEM image (inset of figure 3(b)) shows the distances between the adjacent lattice fringes to be 3.24 Å, a value consistent with the spacing of (321) plans in YAG cubic structure.[43]

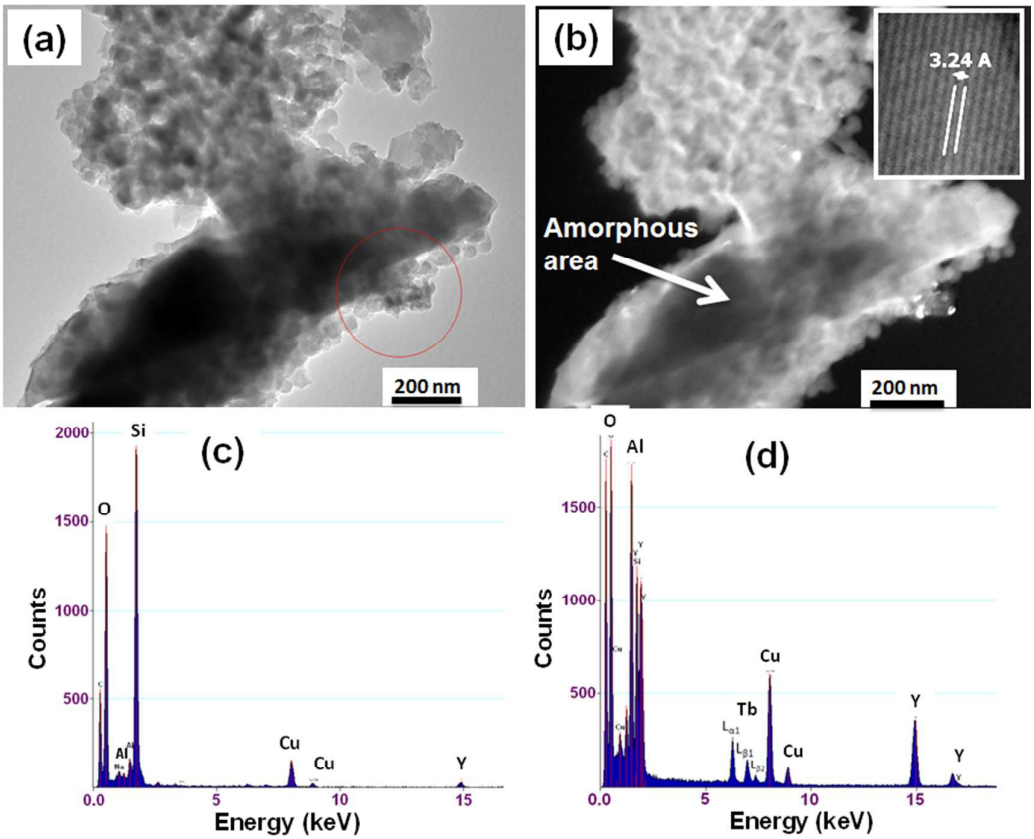

Figure 3. TEM image in (a) bright field mode and (b) dark field mode. EDS spectrum corresponding to (c) an extended zone and (d) a local crystallized zone of MSM-YAG:Tb composite. Inset of figure 3(b) shows HR-TEM image from a crystallized area.

Besides, HR-TEM images taken on grinded MSM-YAG:Tb composite (figure S1, *supporting information*) clearly show discernible YAG:Tb nanoparticles with spherical shape and particle diameter in the range of 20-30 nm, in agreement with crystallite size calculated from XRD pattern. These results confirm that highly crystalline YAG:Tb nanophosphor are synthesized *in situ* inside the pores of MSM and that YAG:Tb nanoparticles are monocrystalline. On the contrary, TEM image of YAG:Tb crystalline powder (Fig. S3) actually shows

highly agglomerated particles with a mean particle size in the range 60-80 nm.

FT-IR spectrum of MSM-YAG:Tb (figure 4(c)) composite shows absorption bands at 785, 728 and 693 cm^{-1} (bands 1, 2 and 3), characteristic of the stretching vibrations of AlO_4 tetrahedra in the $Y_3Al_5O_{12}$ cubic structure. [44, 45] The absorption band at about 570 cm^{-1} (band 5) is attributed to the stretching vibration of AlO_6 octahedra. [45] In addition to these absorption bands, MSM-YAG:Tb composite shows an absorption peak at about 623 cm^{-1} (band 4) which was not observed in YAG:Tb powder. This peak is also due to the Al-O stretching vibration. It could be noticed that this peak was already observed in RE-doped YAG phosphors with particle size smaller than 40 nm and could result from the surface states-related Al species when the surface/volume ratio of the YAG particles is particularly high.[9] Based on these results, it can be concluded that YAG:Tb nanocrystals are formed within the MSM matrix.

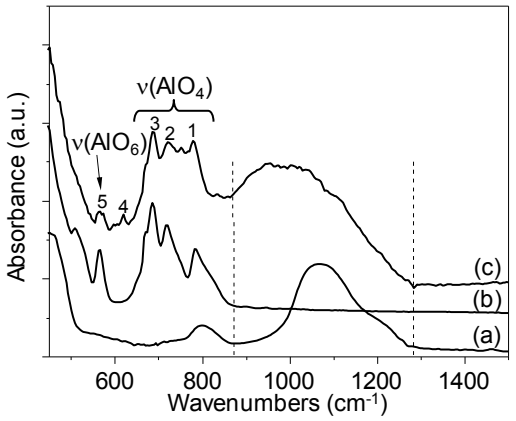

Figure 4. FT-IR spectra of (a) MSM, (b) YAG:Tb phosphor powder and (c) MSM-YAG:Tb composite

By the way, FT-IR spectrum of MSM-YAG:Tb nanocomposite also revealed broader absorption band with a shift to low wavenumbers in the 870-1200 cm^{-1} region when compared to that of MSM monolith. This change most likely results from mixed bands due to Si-O-Si and Si-O-Al linkage.[46, 47] Si-O-Al bond could actually result from the condensation reaction between Si-OH monolith surface groups and Al-OH groups at the surface of YAG:Tb nanocrystals.

Figure 5 shows emission and excitation spectra of MSM-YAG:Tb nanocrystals. The emission and the excitation spectra of YAG:Tb phosphor powder are also shown for comparison. Both YAG:Tb powder and MSM-YAG:Tb nanocomposite exhibit four main PL emission bands, associated with the f-f internal transition from the $^5D_4$ state to the ^7F_J (J = 6, 5, 4, 3, 2) states of Tb^{3+} ions in a crystallized YAG matrix.[48]

Due to the cross-relaxation between $^5D_3$-$^5D_4$ and $^7F_0$-$^7F_6$ of two Tb^{3+}, the blue emission of $^5D_3 \rightarrow {}^7F_J$ is not observed at this doping concentration.[49] For both samples, the $^5D_4 \rightarrow {}^7F_5$ transition (547 nm) is the most intense. Moreover, it can be seen from figure 5 that the PL emission bands of the YAG:Tb crystallized powder are characterized by well-resolved Stark lines, in accordance with the previous reported works.[44] In the case of MSM-YAG:Tb nanocomposite, the emission spectra are almost identical to that of the YAG:Tb crystallized powder but the bands are broader and more characteristic of Tb^{3+} ions dispersed in nano-sized YAG particles.[50, 51] This broadening is generally ascribable to the nanometer-size of the YAG particles. It can be firstly attributed to the fact that fluorescence mainly arises from Tb^{3+} ions located at the nanocrystals surface. The crystallographic sites of these ions are disrupted, leading to very slightly modified PL spectrum when compared with that of regular sites. The shape of the emission bands is also related to the fact that Tb^{3+} ions are embedded in a glass ceramic, resulting in a further inhomogeneous broadening, due to the random stress undergone by the YAG nanocrystals in the pores of silica matrix. It is to be mentioned that similar emission spectra were reported when YAG:Tb nanocrystals were embedded in silica xerogel.[52]

It could be noticed that no wavelength shift was observed when comparing emission bands of MSM-YAG:Tb with those of the YAG:Tb phosphor powder. The main emission band located at 547 nm gave rise to the well-known green luminescence of Tb^{3+} in both cases.The excitation spectra of both samples consist in, at least, three bands in the 250-400 nm wavelength range. The two bands located at shorter excitation wavelength for both YAG:Tb phosphor powder and MSM-YAG:Tb composite are attributed to the 4f→5d ($4f^8 \rightarrow 4f^7 5d^1$) spin-allowed transition (known as low-spin [LS] transition) and spin-forbidden transition (known as high-spin [HS] transition) of Tb^{3+},[53, 54] while the excitation bands located at longer excitation wavelength can be ascribed to the $^7F_6 \rightarrow {}^5D_2$ and $^7F_6 \rightarrow {}^5D_3$ transitions, [55] as shown in table 2.

Moreover, the 5d energy level has a close relationship to the conduction band of the compound. Indeed, due to quantum confinement, smaller crystallites have wider energy band gap. This leads to the 5d energy level change, which is reflected in the blue-shift of the energy of the 4f-5d level due to this size effect.[56]

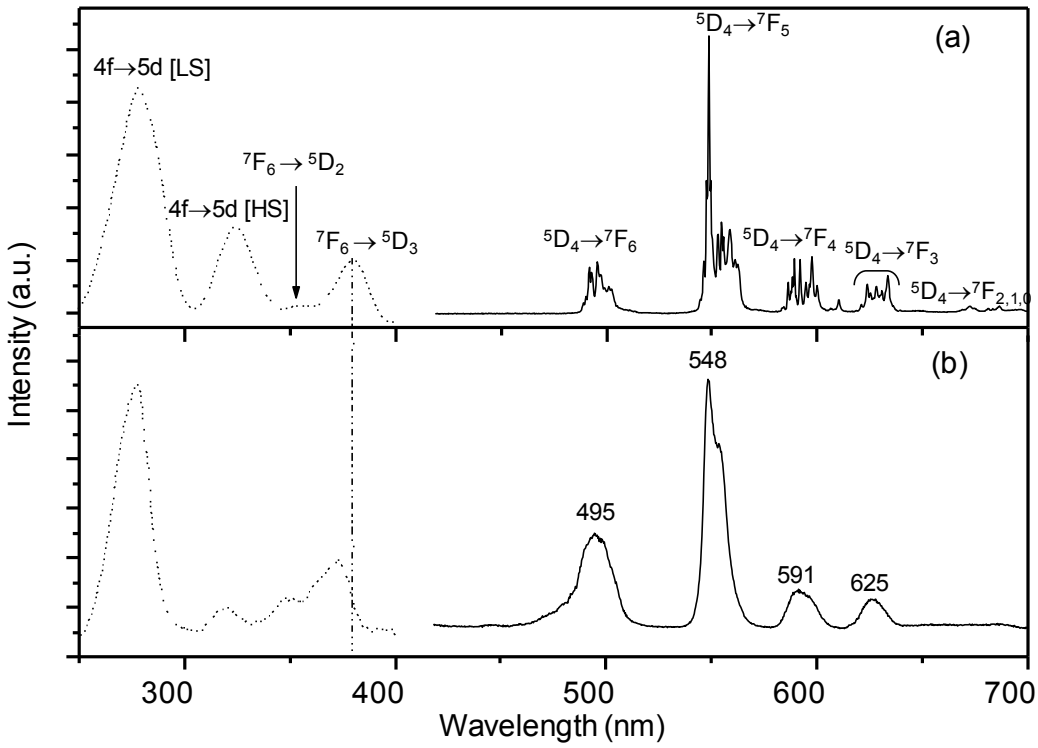

Figure 5. Room temperature PL emission (solid line) and PLE (dotted line) spectra of (a) YAG:Tb phosphor powder and (b) MSM-YAG:Tb nanocomposite. Emission spectra were obtained upon 375 nm excitation. Excitation spectra were recorded with an emission wavelength at 547 nm.From table 2 and figure 5, it can be observed that the excitation bands of MSM-YAG:Tb composite are shifted to shorter wavelengths compared to YAG:Tb crystallized powder. Such effect has already been reported for nanocrystalline YAG:Tb^{3+} phosphor where a blue-shift is observed for the lowest 4f-5d band when compared with the bulk YAG:Tb^{3+} phosphor.[57] This is because the excited states such as 5d are affected by the surrounding electronic shell. In other words, the 5d electrons have a strong interaction with the neighbouring anion ligands in the compound.

Level	$5d^1$ [LS]	$5d^1$ [HS]	$^5D_2$	$^5D_3$
YAG:Tb powder	278	325	355	380
MSM-YAG:Tb	277	319	348	372

Table 2. Excitation wavelength positions (in nm) and corresponding transitions of YAG:Tb powder and MSM-YAG:Tb composite

Figure 6 displays a photograph of a sculpted 30x100 mm piece of MSM-YAG:Tb, before and after excitation at 375 nm, that shows bright and highly homogeneous green emission, in accordance with the homogeneous distribution of YAG:Tb nanocrystals in the silica matrix as shown by TEM images. The MSM-YAG:Tb composite can be easily adorned with LED source to make green luminescent objects with various shapes and sizes for innovative decorative purposes. This approach could also be generalized and applied to various luminescent materials in order to tailor decorative objects depending on the desired colour and shape.

As the YAG:Tb particles in MSM host are nanosized and strongly affected by the surrounding medium, its related PL lifetime is expected to be shorter because the probability of non-radiative recombinations increase in nanocrystals compared to bulk materials, as already reported in the literature for other RE-doped phosphors or phosphors embedded in silica media.[58-61]

Figure 6. Photograph of sculpted piece of MSM-YAG:Tb composite with width/height dimension of 30/100 mm before (right) and after (left) 375 nm excitation.

To confirm this statement, PL decay of the most intense emission wavelength of the Tb^{3+} ions (i.e. 547 nm) in the YAG:Tb powder and MSM-YAG:Tb nanocomposite were both recorded and fitted to a mono-exponential function, as shown in Figure 7. Using these fitted curves, the Tb^{3+} emission lifetimes were calculated to be about 4 and 2.8 ms in the YAG:Tb powder and MSM-YAG:Tb nanocomposite, respectively. This result is thus consistent with our previous statement. It is also in line with PL QY measurements upon 278 nm, which obviously show lower PL QY in the MSM-YAG:Tb composite compared to YAG:Tb powder (about 10% and 35% for MSM-YAG:Tb and YAG:Tb powder, respectively). The shorter PL decay time observed with MSM-YAG:Tb composite supports therefore our assertion that nanosized YAG:Tb phosphor is formed *in situ* in the MSM matrix where YAG:Tb particles have higher surface/volume ratio than YAG:Tb particles in the phosphor powder.

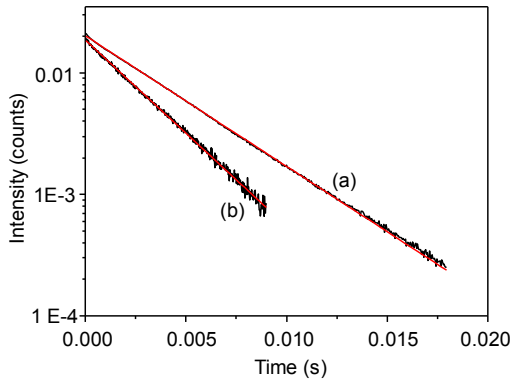

Figure 7. PL decay curves of 547 nm emission of (a) YAG:Tb powder and (b) MSM-YAG:Tb nanocomposite recorded upon 375 nm excitation at room temperature. Red line represents the mono-exponential fit.

Conclusions

In this report, we have demonstrated a successful *in situ* synthesis of highly crystalline YAG:Tb nanophosphor using the pores of MSM as nano-reactors via a simple wet impregnation procedure. MSM host material with mean pore diameter of about 24 nm, prepared using sol-gel method and low-cost silica precursors, was immersed into the YAG:Tb sol. The impregnation process was followed by drying step and annealing process at 1100°C for 4 h. XRD analysis and HRTEM images have obviously showed the formation of highly crystalline YAG:Tb nanocrystals with the YAG cubic structure and crystallite average diameter of about 23 nm. Results also showed an uniform dispersion of YAG:Tb nanocrystals in the MSM matrix, leading to a strong and homogeneous green emission from the composite. The PL properties of MSM-YAG:Tb composite have been discussed and compared to those of neat YAG:Tb phosphor. It was found that excitation spectra are shifted to lower wavelength and PL decay time is significantly shorter in the case of MSM-YAG:Tb composite compared to the neat YAG:Tb phosphor. Moreover, PL emission spectra from MSM-YAG:Tb nanocomposite showed broader emission bands when compared to those of YAG:Tb powder. These results are in line with the formation of nano-sized YAG:Tb phosphor within the MSM host matrix. The method we developed in the present work can obviously be applied, as a versatile procedure, to a large variety of materials (oxides, fluorides, etc.) synthesized by the sol-gel route. A large size (30x100 mm) of sculpted MSM-YAG:Tb composite was successfully designed and promises a huge potential to be applied in decorative lighting.

Acknowledgements

The authors thank Elisabeth Hans (Jewellery, creation and design realization) for the sculpture realized on the MSM-YAG:Tb piece (www.ehans-joailler.com). Research on sol-gel silica monoliths was partly supported by the "Fonds Européen de Développement Economique Régional" and the Labex CEMPI and Equipex FLUX through the "Programme Investissements d'Avenir". The TEM facility in Lille (France) is supported by the Conseil Régional du Nord-Pas de Calais, and the European Regional Development Fund (ERDF).

Notes and references

[1] *Université Clermont Auvergne, Université Blaise Pascal, Institut de Chimie de Clermont-Ferrand, BP 10448, F-63000 CLERMONT-FERRAND, FRANCE*

[2] *CNRS, UMR 6296, ICCF, F-63171 AUBIERE, FRANCE*

[3] *Laboratoire de Physique des Lasers, Atomes et Molécules (PhLAM), CNRS (UMR 8523), CERLA/IRCICA, Université Lille 1-Sciences et Technologies, UFR de Physique, Bâtiment P5, F-59655 VILLENEUVE D'ASCQ cedex, FRANCE*

[4] *Université Clermont Auvergne, ENSCCF, Institut de Chimie de Clermont-Ferrand, BP 10448, F-63000 CLERMONT-FERRAND, FRANCE*

*Corresponding Author: *E-mail: Genevieve.chadeyron@ensccf.fr*

Electronic Supplementary Information (ESI) available: [Figures S1 and S2 show high magnification and high resolution TEM images of grinded MSM-YAG:Tb composite. Figure S3 exhibits a TEM image of the YAG:Tb crystallized powder.]. See DOI: 10.1039/b000000x/

1. S. Shionoya, W. M. Yen and H. Yamamoto, *Phosphor Handbook*, CRC Press, 2006.
2. C. C. Lin and R.-S. Liu, *J. Phys. Chem. Lett.*, 2011, **2**, 1268-1277.
3. S. Ye, F. Xiao, Y. X. Pan, Y. Y. Ma and Q. Y. Zhang, *Mater. Sci. Eng. R*, 2010, **71**, 1-34.
4. A. Aboulaich, M. Michalska, R. Schneider, A. Potdevin, J. Deschamps, R. Deloncle, G. Chadeyron and R. Mahiou, *ACS Appl. Mater. Interfaces*, 2014, **6**, 252-258.
5. Y.-C. Lin, J. P. You, N. T. Tran, Y. He and F. G. Shi, *Journal of Electronic Packaging*, 2011, **133**, 011009-011009.
6. N. Bardsley, S. Bland, D. Chwastyk, C. d. Monasterio, L. Pattison, M. Pattison, F. Welsh and M. Yamada, U.S Department of Energy, 2013.
7. S. C. Huang, J. K. Wu, W.-J. Hsu, H. H. Chang, H. Y. Hung, C. L. Lin, H.-Y. Su, N. Bagkar, W.-C. Ke, H. T. Kuo and R.-S. Liu, *Int. J. Appl. Ceram. Technol.*, 2009, **6**, 465-469.
8. L. Chen, C.-I. Chu and R.-S. Liu, *Microelectronics Reliability*, 2012, **52**, 900-904.
9. A. Aboulaich, J. Deschamps, R. Deloncle, A. Potdevin, B. Devouard, G. Chadeyron and R. Mahiou, *New J. Chem.*, 2012, **36**, 2493-2500.
10. D. Jia, *Chem. Eng. Commun.*, 2007, **194**, 1666-1687.
11. D. Jia, *Electrochem. Solid-State Lett.*, 2006, **9**, H93-H95.

12. D. Jia, Y. Wang, X. Guo, K. Li, Y. K. Zou and W. Jia, *J. Electrochem. Soc.*, 2007, **154**, J1-J4.
13. L. T. Su, A. I. Y. Tok, Y. Zhao, N. Ng and F. Y. C. Boey, *J. Phys. Chem. B*, 2009, **113**, 5974--5979.
14. N. Pradal, G. Chadeyron, A. Potdevin, J. Deschamps and R. Mahiou, *J. Eur. Ceram. Soc.*, 2013, **33**, 1935-1945.
15. S. Das, A. Amarnath Reddy, S. Ahmad, R. Nagarajan and G. Vijaya Prakash, *Chem. Phys. Lett.*, 2011, **508**, 117-120.
16. A. Bao, H. Yang and C. Tao, *Curr. Appl. Phys.*, 2009, **9**, 1252-1256.
17. S. S. Pitale, V. Kumar, I. Nagpure, O. M. Ntwaeaborwa and H. C. Swart, *Curr. Appl. Phys.*, 2011, **11**, 341-345.
18. J. Liao, H. You, B. Qiu, H.-R. Wen, R. Hong, W. You and Z. Xie, *Curr. Appl. Phys.*, 2011, **11**, 503-507.
19. F. Hoffmann, M. Cornelius, J. Morell and M. Fröba, *Angew. Chem., Int. Ed.*, 2006, **45**, 3216-3251.
20. S. J. Lee, S. H. Park Ss Fau - Lee, S.-H. Lee Sh Fau - Hong, C.-S. Hong Sh Fau - Ha and C. S. Ha, *J. Nanosci. Nanotechnol.*, 2013, **13**, 7459-7466.
21. A. Feinle, F. Lavoie-Cardinal, J. Akbarzadeh, H. Peterlik, M. Adlung, C. Wickleder and N. Hüsing, *Chem. Mater.*, 2012, **24**, 3674-3683.
22. N. Brun, B. Julián-López, P. Hesemann, G. Laurent, H. Deleuze, C. Sanchez, M.-F. Achard and R. Backov, *Chem. Mater.*, 2008, **20**, 7117-7129.
23. Y. Du, Y. Fu, X. Guo, H. Li, C. Lü and Z. Su, *Microporous Mesoporous Mater.*, 2010, **130**, 122-129.
24. Q. Meng, L. Fu, J. Lin, H. Zhang, S. Wang, Y. Zhou, M. Yu and F. Liu, *J. Phys. Chem. Solids*, 2003, **64**, 63-67.
25. C. Stan, N. Marcotte, M. Secula and M. Popa, *J. Sol-Gel Sci. Technol.*, 2014, **69**, 207-213.
26. X. Gao and S. Nie, *J. Phys. Chem. B*, 2003, **107**, 11575-11578.
27. J. Yang, Y. Deng, Q. Wu, J. Zhou, H. Bao, Q. Li, F. Zhang, F. Li, B. Tu and D. Zhao, *Langmuir*, 2010, **26**, 8850-8856.
28. L. Sorensen, G. F. Strouse and A. E. Stiegman, *Adv. Mater.*, 2006, **18**, 1965-1967.
29. Y. Chen, Q. Chen, L. Song, H.-p. Li and F.-z. Hou, *Microporous Mesoporous Mater.*, 2009, **122**, 7-12.
30. Y. J. Gu and B. Yan, *J. Colloid Interface Sci.*, 2013, **393**, 36-43.
31. Y. Chen, Q. Chen, L. Song, H.-p. Li and F.-z. Hou, *J. Alloys Compd.*, 2010, **490**, 264-269.
32. H. Xu, L. Cheng, C. Wang, X. Ma, Y. Li and Z. Liu, *Biomaterials*, 2011, **32**, 9364-9373.
33. Y.-F. Han, F. Chen, Z. Zhong, K. Ramesh, L. Chen and E. Widjaja, *J. Phys. Chem. B*, 2006, **110**, 24450-24456.
34. T. Takayuki, H. Manabu, D. Hiroyuki, M. Masaki, K. Atsushi and K. Shigemi, *Jpn. J. Appl. Phys.*, 2010, **49**, 06GH04.
35. G. D. Mihai, V. Meynen, M. Mertens, N. Bilba, P. Cool and E. F. Vansant, *J Mater Sci*, 2010, **45**, 5786-5794.
36. Z. Li, H. Zhang and H. Fu, *J. Lumin.*, 2013, **135**, 79-83.
37. A. Potdevin, G. Chadeyron, D. Boyer and R. Mahiou, *J Mater Sci*, 2006, **41**, 2201-2209.
38. H. El Hamzaoui, L. Courthéoux, V. N. Nguyen, E. Berrier, A. Favre, L. Bigot, M. Bouazaoui and B. Capoen, *Mater. Chem. Phys.*, 2010, **121**, 83-88.
39. A. Potdevin, G. Chadeyron and R. Mahiou, *Chem. Phys. Lett.*, 2010, **490**, 50-53.
40. S. Brunauer, P. H. Emmett and E. Teller, *J. Am. Chem. Soc.*, 1938, **60**, 309-319.
41. E. P. Barrett, L. G. Joyner and P. P. Halenda, *J. Am. Chem. Soc.*, 1951, **73**, 373-380.
42. B. D. Cullity and S. R. Stock, *Elements of X-Ray Diffraction, 3rd Edition*, Prentice Hall, 2001.
43. A. Nakatsuka, A. Yoshiasa and T. Yamanaka, *Acta Crystallogr., Sect. B: Struct. Sci.*, 1999, **55**, 266-272.
44. J. A. Koningstein, *Chem. Phys. Lett.*, 1969, **3**, 303-304.
45. O. Yamaguchi, K. Takeoka, K. Hirota, H. Takano and A. Hayashida, *J Mater Sci*, 1992, **27**, 1261-1264.
46. P. Padmaja, G. M. Anilkumar, P. Mukundan, G. Aruldhas and K. G. K. Warrier, *Int. J. Inorg. Chem.*, 2001, **3**, 693-698.
47. P. Kansal, R. M. Laine and F. Babonneau, *J. Am. Ceram. Soc.*, 1997, **80**, 2597-2606.
48. A. Potdevin, G. Chadeyron, V. Briois, F. Leroux and R. Mahiou, *Dalton Trans.*, 2010, **39**, 8718-8724.
49. N. Bodenschatz, R. Wannemacher, J. Heber and D. Mateika, *J. Lumin.*, 1990, **47**, 159-167.
50. H.-h. Kwak, S.-J. Kim, H.-H. Yoon, S.-J. Park and H.-w. Choi, *J Electroceram*, 2009, **23**, 397-401.
51. J. Zhou, F. Zhao, X. Wang, Z. Li, Y. Zhang and L. Yang, *J. Lumin.*, 2006, **119–120**, 237-241.
52. M. Kubus, H. J. r. Meyer, L. Kienle and A. M. Klonkowski, *J. Non-Cryst. Solids*, 2009, **355**, 1333-1337.
53. A. Potdevin, G. Chadeyron, D. Boyer and R. Mahiou, *J. Appl. Phys.*, 2007, **102**, 073536-073536.
54. J. Y. Choe, D. Ravichandran, S. M. Blomquist, K. W. Kirchner, E. W. Forsythe and D. C. Morton, *J. Lumin.*, 2001, **93**, 119-128.
55. Z. Zhang, O. M. ten Kate, A. Delsing, E. van der Kolk, P. H. L. Notten, P. Dorenbos, J. Zhao and H. T. Hintzen, *J. Mater. Chem.*, 2012, **22**, 9813-9820.
56. Y. Hakuta, T. Haganuma, K. Sue, T. Adschiri and K. Arai, *Mater. Res. Bull.*, 2003, **38**, 1257-1265.
57. S. Zhou, Z. Fu, J. Zhang and S. Zhang, *J. Lumin.*, 2006, **118**, 179-185.
58. P. Packiyaraj and P. Thangadurai, *J. Lumin.*, 2014, **145**, 997-1003.
59. H. Peng, H. Song, B. Chen, J. Wang, S. Lu, X. Kong and J. Zhang, *J. Phys. Chem.*, 2003, **118**, 3277-3282.
60. R. Hansel, S. Allison and G. Walker, *MRS Proceedings*, 2008, **1076**, K06.
61. R. S. Meltzer, S. P. Feofilov, B. Tissue and H. B. Yuan, *Phys. Rev. B*, 1999, **60**, R14012-R14015.